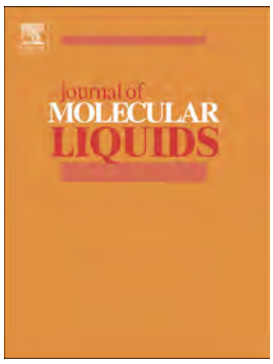

Low temperature dependence of protein-water interactions on barstar surface: A nano-scale modelling

M.C. Morón

PII: S0167-7322(18)34613-0
DOI: doi:10.1016/j.molliq.2018.10.041
Reference: MOLLIQ 9786

To appear in: *Journal of Molecular Liquids*

Received date: 6 September 2018
Accepted date: 8 October 2018

Please cite this article as: M.C. Morón , Low temperature dependence of protein-water interactions on barstar surface: A nano-scale modelling. Molliq (2018), doi:10.1016/j.molliq.2018.10.041

Your reference: MOLLIQ 9786
Article reference: MOLLIQ_2018_4441
Article title: Low temperature dependence of protein-water interactions on barstar surface: a nano-scale modelling
To be published in: Journal of Molecular Liquids

6 September 2018

Low temperature dependence of protein-water interactions on barstar surface: a nano-scale modelling

M. C. Morón [a,b]

[a] *Instituto de Ciencia de Materiales de Aragón (ICMA), Consejo Superior de Investigaciones Científicas-Universidad de Zaragoza, Pedro Cerbuna 12, E-50009 Zaragoza, Spain. E-Mail: nina@unizar.es.*
[b] *Departamento de Física de la Materia Condensada, Facultad de Ciencias, Universidad de Zaragoza, Zaragoza, Spain.*

Corresponding author:
M. C. Morón
Instituto de Ciencia de Materiales de Aragón
Universidad de Zaragoza
Pedro Cerbuna 12
E-50009 Zaragoza
Spain
E-mail: nina@unizar.es
E-mail: oenola@gmail.com

Abstract

The dynamics of the hydration shell of the inhibitor barstar is analysed at low temperature (300 – 243 K), through all-atom molecular dynamics simulations, and compared with that of bulk water. The relaxation of residence times of solvent molecules in the protein hydration shell follows a stretched exponential function $exp[-(t/\tau)^{\beta}]$ with $\beta=0.48\pm0.01$, independent of temperature, showing that the decay process is mainly dominated by long-range molecular relaxation channels (short-range for bulk water). The percentage of water molecules exhibiting 4 hydrogen bonds, x^{HB4}, is found to be a parameter essential for understanding some room and low temperature dependent properties of the protein hydration shell, suggesting an explanation for the unfreezing of protein hydration water as temperature decrease below 273 K. Moreover the dynamical transition that proteins and their hydration water exhibit at ~225 K can be explained by the decrease of 'hydrogen bond defects' in the protein hydration shell as temperature goes down. If most of those water molecules would present a tetrahedral arrangement (nearly no 'hydrogen bond defects'), the bioactivity of proteins would be negligible. Comparison with experimental results is provided all along the work. Experimental data are quantitatively reproduced.

Keywords

Protein hydration water dynamics; Hydrogen bond network; Bulk water dynamics; Low temperature; Relaxation phenomena; All-atoms molecular dynamics simulations

1. Introduction

The protein hydration shell is fundamental to protein structure, dynamics, and function. Although water is one of the simplest molecules, it plays an utmost and ubiquitous role on Earth and in all aspects of life. Understanding its properties is of fundamental importance in science and technology. Thus water is essential in biology, because it participates in nearly every process necessary for life [1-3]. In native scenarios, proteins are typically in close contact with water solutions. The shell of water molecules in close interaction with the protein surface is usually called protein hydration water but also biological water [4-5]. That particular water is involved in biochemical processes such as protein folding, enzyme function, molecular recognition or amyloid beta aggregation (Alzheimer's disease) [6-11]. In fact in the dehydrated state, the function of proteins is severely impeded [12]. The knowledge of the structure and dynamics of water molecules in the so-called hydration layer surrounding proteins is therefore of absolute relevance to the understanding of the protein functionality [13-15]. Thus hydration water should not be treated as a simple solvent, but rather as an active component of biomolecular systems [16].

Reciprocally both experimental [9,17] and simulation results [18-20] agree on that a protein perturbs the water dynamics in its hydration shell. However the degree and molecular origin of this perturbation are not yet completely understood [4,21]. Water molecules in the protein hydration layer can be considered to be spatially confined. This water is expected to behave differently from the bulk because of the interaction with protein residues. If macroscopic data are considered (i.e. relaxation times), the dynamics of biological water is affected only to a small extent (2-4-fold slowdown) when compared with neat water [14,22,23]. However if microscopic data are taken into account, that hydration water dynamics exhibits a slow component neatly smaller than that of bulk water (2-3 orders of magnitude) [24-26]. The magnitude and molecular origin of this retardation are still topics for further study [26-29]. Moreover some authors state that the heterogeneous scenario biological water presents is due to the heterogeneity of the protein surface itself in contrast to the more homogeneous nature of the solvent, suggesting that the hydrogen-bond dynamics between the protein and the hydration water is governed by the protein [30].

On the other hand in structural studies and many commercial applications, proteins are increasingly exposed to low temperatures. The role of solvents in biomolecular dynamics is another important topic that is directly related to the field of bio-cryopreservation. Thus in hydrated proteins, water molecules directly in contact with, or close to, the protein surface are not able to crystallize and form ice, usually they are still in the liquid state below the melting point of bulk water [31]. Exact requirements for avoiding crystallization are difficult to provide. Moreover many experimental studies have examined the thermal limit of the biological activity of proteins and have related its onset at low temperatures to the existence of a dynamical crossover in the hydration water at approximately 225 K [32,33]. Although this precise value of temperature has been questioned, due to a possible inadequate instrumental resolution, there is a consensus that the crossover exists and that it is relevant [34]. Interestingly enough, proteins have been also reported to present a 'dynamical transition' at that temperature [35]. Recently a simple but effective computational method to predict physical magnitudes of bulk water at low temperature, in quantitative agreement with experimental results, has been published [26]. It would be of interest to examine if that

method could be also successfully applied to protein hydration water at low temperatures.

In this work we explore such scenarios analysing in detail some aspects of the dynamics of the hydration water around the protein barstar, in particular the low temperature dependence of protein-water interactions at protein surface. The influence of the protein on the dynamics of its hydration water is considered, but also the opposite, the effect of water dynamics on the biomolecule. Differences and similarities between protein hydration water and bulk water are also examined. Moreover this work analyses at nanoscopic level, the impact of the percentage of water molecules presenting four hydrogen bonds, either with the protein or with the solvent, on the dynamics of the protein hydration water. On the other hand barstar is a ribonuclease inhibitor that can be found in *Bacillus amyloliquefaciens*. It is an 89-residue protein of interest in molecular recognition (drug discovery) [36], cancer cell research [37] and amyloid fibrils investigations (neurodegenerative diseases) [38]. In order to follow the dynamics and existing interactions between the protein and its hydration water at nanoscopic level, we have carried out all-atoms molecular dynamics simulations at room and low temperature. Those numerical simulations are very useful for providing details of dynamical processes that are not experimentally reachable [25,39-40].

The paper is organized as follows. Section 2 presents the details of the computer simulations carried out on the inhibitor barstar in a bath of water molecules at different temperatures from ambient down to 243 K. In section III the dynamics of the protein hydration water is analysed through relaxation processes, temporal distributions (residence times) and hydrogen bond analysis. Those results are discussed in Section 4 and compared with previously reported experimental and simulated data as well as theoretical models. The main conclusions are summarised in Section 5.

2. Materials and Methods

Classical all-atom molecular dynamics simulations of aqueous solutions of the protein barstar (wild type) were conducted at 300 K [25], 288 K, 273 K, 258 K, 248 K and 243 K. The initial structure of that inhibitor was obtained from the RCSB Protein Data Bank (PDB ID: 1BRS). The water molecules shown in the crystallographic PDB data were not maintained. The simulations were performed using the GROMACS software package in double precision [41,42]. After adding the hydrogens, the whole protein was immersed in a large cubic box, 6.2 nm along the three axes, of well equilibrated water by carefully avoiding unfavourable contacts. The periodic boundary condition was applied in order to prevent boundary effects. That procedure produced a system containing 1432 protein atoms and 7430 water molecules. In order to eliminate possible unfavourable interactions between the solute and the solvent, the energy of the system was minimized using steepest descent and conjugate gradient algorithms implemented in the Gromacs software package [41,42]. Conjugate gradient is slower than steepest decent in the early stages of the minimization, but becomes more efficient closer to the energy minimum. The minimization was stopped when the maximum force reached a value smaller than 1.0 kJ mol^{-1} nm^{-1}. The interactions between the constituents of the system were described employing a multi-component all-atom force field (OPLS-AA) [43,44]. All bond lengths were constrained using the LINCS algorithm [45]. The cutoff length for the Lenard-Jones and Coulomb potentials was set

at 1.4 nm. The simulations were performed using a time step (resolution) of 2 fs (0.002 ps).

In the present work the residence times of water molecules at the surface of the protein barstar are calculated together with the number of hydrogen bonds that special kind of water exhibits. We aim to compare our room and low temperature results with those obtained for bulk water. In a previous work [26] we have determined those magnitudes for neat water, reproducing experimental data even at low temperature. In order to performed a quantitative comparison between protein hydration and bulk water, it is important to use the same protocol, for simulations and calculations, in both cases. Thus the molecular dynamics simulations (present work) use the three site simple point charge model (SPC) [46] for moldelling water, as do the previous reported research concerning bulk water [26]. As in that publication [26], the computer simulations we show (present work) were performed using the Langevin equation of motion $m(d^2r/dt^2) = F - \gamma(dr/dt) + \eta(t)$, where *m*, r and F are, respectively, the mass, the position and the force field acting on the atom under consideration in the dynamics. $\eta(t)$ is a noise term with correlation function $< \eta_i(t) .\eta_j(t')> = 2k_BT(m/taut)\delta_{i,j}\delta(t-t')$ [41,42]. $\gamma = m/taut$ is the damping factor where *taut* is the coupling constant time obtained from reference [26] for each temperature. After an equilibration period, the trajectories for data production were performed in the canonical ensemble, i.e. at constant N, V and T, saving the production runs every 0.1 ps for later analysis. In order to reach a correct stabilization of the simulated systems, the equilibration times were varied for different temperatures from a few nanoseconds at 300 K to tens of nanoseconds at 243 K. The trajectories of the atoms were monitored during 7 ns for simulations at 300 K, 288 K and 273 K, 10 ns at 258 K, 13 ns at 248 K and 35 ns at 243 K. Those particular temperature values were chosen in order to compare with previous data for bulk water [26]. During those production runs the root mean square deviation of the inhibitor barstar was found to maintain a regular value (around 0.20 nm) with respect to its initial configuration indicating an equilibrated state. The error bar for all the temperatures considered in this work is ± 1 K.

3. Results

The dynamics of ambient and low temperature hydration water around the inhibitor barstar is analysed in this section through relaxation processes, temporal distributions (residence times) and hydrogen bond calculations.

3.1. Relaxation phenomena

The dynamics of water can be described by evaluating, as a function of time, the occupation of the water molecules on a given spatial arrangement (i.e. a spherical region). That occupancy is related to the mobility (diffusion coefficient) of the water molecules through the region considered. Thus we have considered the decay equation

$$D(t) = \sum_{i=1}^{N} [< O_i(t_o)O_i(t_o + t\ ) > / < O_i(t_o\ )O_i(t_o\ ) >]$$

where $O_i(t_o+t)$ takes the value of 1 (unity) if the water molecule *i*, which is within the region of interest at the time origin t_o, still exists in that region at time $t_o + t$ [26,47-51]. Otherwise $O_i(t_o + t)$ equals 0. N is the total number of water molecules within the region considered at t_o. The angular brackets denote averaging over various time origins with the aim of improving statistics as well as taking into account different areas of the trajectory. Therefore *D(t)* calculates the average number of water molecules that still remain in the region of interest after a simulation time *t*. In order to analyse the first hydration layer around the protein, we have calculated that magnitude for water molecules that are present within a shell of thickness 0.40 nm from all atoms of the biomolecule, hydrogen excluded (see Fig. 1). Larger radius will result in taking into account more of the bulk dynamics. It is also the thickness that has been already considered in previous data at ambient temperature [25].

The magnitude *D(t)* was calculated with a resolution of 0.1 ps, using the data obtained from all-atom molecular dynamics simulations at 288 K, 273 K, 258 K, 248 K, and 243 K (as an example see Fig. 2). The tendency of the curves consists of a fast initial decay followed by a slower one. This trend cannot be described using a single exponential law. Instead a stretched exponential function $exp[-(t / \tau)^{\beta}]$ has been used to fit the data (see Fig. 2) [52,53]. This function, which contains just two free parameters: the effective relaxation time τ and the stretching exponent β ($0 < \beta \leq 1$), was proposed empirically more than 150 years ago for its accuracy and simplicity in describing decay data. The stretched exponential, also known as the KWW (Kohlraush-Williams-Watts) function, is often observed in several phenomena in complex condensed matter systems and supercooled liquids [54].

The fit of our data to that expression supplies parameter values τ and β that are shown in Table 1 as a function of the temperature. The time constant τ gives an estimation of the permanence time of water molecules in the solvent region under study, providing the overall time scale over which the process develops. A particular behaviour arises from the stretched exponent since the value of that parameter nicely keeps constant from 300 to 243 K ($\beta = 0.48 \pm 0.01$) indicating an independence of the KWW exponent β with temperature (see Fig. 3, lower inset).

The exponent of the KWW function also provides interesting information as for example how large is the deviation of the relaxation curve from a classical exponential since for $\beta = 1$ the mathematical expression of a simple exponential is restored. In our case, the large stretching effect ($\beta \approx 0.5$), both at room and low temperature, indicates a considerable large deviation from a classical exponential decay showing that water dynamics in the temperatures considered is characterized by, not a unique relaxation time (since $\beta \neq 1$), but a distribution of different time scales. That finding suggests the presence of significant temporal disorder in the system [54,55]. Stretched exponentials are frequently employed for modelling phenomena characterized by multiple relaxation rates [56].

In addition the exponent $\beta = 0.48 \pm 0.01$ is in excellent agreement with experimental determinations. Thus quasi-elastic neutron scattering experiments performed on water molecules located at the surface of the protein c-phycocyanin indicate a stretched exponential parameter $\beta \approx 0.5$ at 293 K [57]. Same experimental technique applied to the hydration shell of protein lysozyme shows an independent temperature exponent $\beta =$

0.5 [35], as also does water confined in laboratory synthesized nanoporous silica matrices with pore diameters of 1.8 and 1.4 nm ($\beta \approx 0.5$) [58].

The previous paragraphs show that, in the range considered, the stretched exponent β is independent of the temperature. What about the thermal dependence of the other stretched parameter, the relaxation time τ? In this paragraph the increase of the relaxation time τ as the temperature decreases is analysed with more detail. Thus, the evolution of the effective relaxation time τ with the temperature is shown in Fig. 3 (upper inset). The increase of τ as the temperature decreases has been fitted to the expression $\tau \sim (T - T_L)^{-\gamma}$. The result is showed in Fig. 3 where a nice linear dependence is found for the evolution of $\tau^{-(1/\gamma)}$ with temperature. The best fit corresponds to $T_L = 226 \pm 4$ K and $\gamma = 1.8 \pm 0.2$ in good agreement with the results also obtained from τ values (residence times) for bulk water: $T_{bulkwater} = 227 \pm 3$ K and $\gamma = 1.71 \pm 0.1$ [26]. These results, virtually the same for both neat and biological water, show that the dynamic crossover phenomenon in protein hydration water is an intrinsic property of isolated water, and is not due to the spatial confinement scenario. Our result for the crossover temperature T_L, also agrees with those obtained for the hydration water of the protein lysozyme from nuclear magnetic resonance (NMR) [32], quasielastic neutron scattering (QENS) [33] and molecular dynamics simulations (self-diffusion constant and self-intermediate scattering function) [59] that provide values $T_L = 225 \pm 5$ K and $\gamma = 1.8$, $T_L = 225 \pm 5$ K and $T_L = 223 \pm 2$ K, respectively. It also agrees with $T_L = 200$-230 K, a result obtained for trp-cage mini-protein hydration water, by computing mean square displacements [60]. The convergence of all those results supports the existence of a crossover occurring in the hydration layer of the protein barstar in consonance with that occurring at a similar temperature for bulk water. Interestingly enough, the low temperature thermal limit of biological activity of a protein has been linked to the occurrence of a dynamical crossover in the hydration water of the biomolecule at $T_L \approx 225$ K [34].

3.2 Distribution of residence times

To gain an atomic level understanding of the observed distribution of times associated to the stretched relaxation we have analysed in section 3.1, we calculated the residence times that water molecules exhibit around a given environment (atom) of the inhibitor barstar. The purpose was to use the molecular dynamics simulations as an atomic resolution instrument. Therefore the attention was focused on different atoms of the protein (more than 50 snapshots were analysed) in order to see if the structural images could illustrate and corroborate at atomic level the existence of various time scales as suggested in the previous section 3.1 for protein hydration water. As an example, two of the most representative snapshots are depicted in Figs. 4 and 5. Those figures show the heterogeneous distribution of residence times of solvent molecules residing at a distance smaller than 0.40 nm i) from the oxygen atom (carboxyl group) of the non-polar residue Alanine36 at 300 K and ii) from the oxygen atom (hydroxyl group) of the polar residue Threonine19 at 243 K (see Fig. 1). A wide distribution of residence times can be observed. Please mind that the interest of those snapshots is not the particular distribution of times_but the atomic level illustration of the multi-time dynamics of the first hydration shell around barstar when decreasing the temperature from ambient to 243 K.

With the aim of scrutinising a global picture, the time that the 7430 solvent molecules of the simulations spend at a distance smaller than 0.40 nm from all the atoms integrating the protein, hydrogens excluded, has been calculated from 300 K down to 243 K. The results are shown in Fig. 6 for the extreme temperatures. A heterogeneity of residence times (t_r) is detected along the whole temperature range. The longest residence times found at 300 K amounts some units of nanoseconds while those at 243 K increase up to some tens of nanoseconds (see Fig. 6). The difference between those room and low temperature values is one order of magnitude. Same calculations performed for the intermediated temperatures reported above (300 - 243 K) agree with the nanoscopic slowing of the dynamics of biological water as temperature decreases. Slow hydration water is interesting for several reasons. It retards charge transfer processes [61,62], prevents dehydration [61], and increases friction on the surface involved [63]. Moreover slow confined clusters of water molecules also play a central role in protein function, including allosteric regulation and charge transfer [64,65]. Water molecules involved in bridging proteins and single-stranded DNA molecules have been reported to form a highly constrained thin layer with extremely retarded mobility [66].

Same calculations performed for bulk water, following the same procedure and simulation protocol than that of the present work, show that the largest residence times found at 300 K amounts some tens of picoseconds while those at 243 K increases up to some hundreds of picoseconds [26]. The difference is about one order of magnitude, as in the case of protein hydration water.

As an example, Fig. 7 shows one of the slowest water molecules located in the hydration shell of the inhibitor barstar. That solvent molecule spends more than 2 ns at room temperature (300 K) and more than 20 ns at low temperature (243 K) in the pocket defined by the residues Pro48, Leu49, Val50, Asp83, Ile84 and Thr85. These residues are located at two of the three beta strands of barstar (see Fig. 7). The position of that special solvent molecule coincides with that of one crystallization water molecule, identified with the number 202, in the crystal structure of the protein (Protein Data Bank, code 1brs).

3.3 Scale-free dynamics

Since the appearance of stretched exponentials can be related to the spread in the residence time values indicating complex time scales [67], the number of water molecules that spend a given time t_r within the already considered cutoff of 0.40 nm from the protein has been calculated as $N_{biowater}(t_r)$ for 300 [25], 288, 273, 258 and 243 K. If the evolution of $N_{biowater}(t_r)$ with t_r is represented in a double-logarithm plot, a straight line is obtained (see Fig. 8 for T = 288 and 243 K). This result shows that the temporal distribution of the water molecules within the first hydration layer (cutoff 0.40 nm) of the protein barstar follows a power law, $N_{biowater}(t_r) \sim t_r^{-\alpha}$ for at least three decades (0.1 – 100 ps) both at room and low temperature. If the exponent α were unity, there would be one water molecule spending 100 ps within the hydration water of the protein for every 100 solvent molecules spending 1 ps. The fact that the distribution begins to deviate from a straight line at high times is a finite-size effect [68].

We have obtained a temperature independent exponent $\alpha = 0.63 \pm 0.07$. The negative sign of the slope indicates that most of the water molecules stay during short periods of

time near the protein, while few of them spend much longer times, reflecting heterogeneity in the temporal behaviour of hydration water. The existence of that power law for at least three decades shows that biological water displays the same type of distribution at any scale, i.e., it is scale-free [69]. That behaviour is maintained as the temperature decreases down to at least 243 K. Some empirically observed networks have been reported as scale free: social, computer or biological networks [69]. Our work presents a scale-free distribution in time with the agents at atomic level (water molecules). On the other hand Leitner and co-workers, in a theoretical work performed at room temperature, have reported a power law scaling for the energy flow dynamics in proteins as myoglobin and green fluorescent protein, with positive slopes amounting 0.58 and 0.6, respectively [70,71]. In both cases the power law holds for one decade (0.1 - 3 ps).

At that point a question arises: would bulk water also present a scale-free behaviour with respect to the residence times of solvent molecules? In order to answer that question, the number of water molecules that spend a given time t_r within a spherical region has been calculated as $N_{bulkwater}(t_r)$. With the aim of improving statistics we have calculated that function for bulk water molecules located within a sphere with a radius of 2.0 nm that was centred in the simulation box. Moreover that cutoff approximates the diameter of some small proteins of interest plus its first hydration shell [25,72]. All these calculations have been performed using all-atom molecular dynamics simulations carried out on bulk water at 300, 288, 273, 258 and 243 K [26], following the same simulation protocol than that used in the present work.

At room temperature if the evolution of $N_{bulkwater}(t_r)$ with t_r is represented in a double-logarithm plot, a straight line is obtained (see Fig. 9). These data demonstrate that the distribution of the water molecules within the cutoff of reference follows a power law, $N_{bulkwater}(t_r) \sim t_r^{-\alpha}$, where t_r stands for the residence time that different solvent molecules spend within that sphere. We find a slope of $\alpha = 0.50 \pm 0.04$ at 300 K. A value $\alpha = 0$ would evidence a homogeneous distribution of residence times. The power law scaling shows that a characteristic single residence time does not exist but a distribution of times. Thus the presence of that power law reflects the existence of heterogeneity in the temporal behaviour of bulk water. Such behaviour can be also found if the radius of the sphere considered is changed (i.e. 1.5 and 1.0 nm). Martiniano and Galamba have studied hydrogen bond lifetime probability distributions for bulk water using molecular dynamics simulations [39]. They report the existence of a power law along one decade (0.1 – 1 ps). These authors suggest that the power law decay would be related to librational and translational motions that take place on the time scale of hydrogen bond breaking/re-forming.

The results shown in Fig. 9, a power law behaviour holding at least for three decades (0.1 -100 ps), let to conclude that room temperature bulk water displays the same type of distribution at any scale, i.e., it is scale-free (with respect to the residence time of solvent molecules) [69]. Therefore the identification of bulk water as exhibiting a scale-invariant dynamics opens the possibility of applying all the mathematical and physical knowledge that has been already developed for scale-free systems [69,73] to this particular solvent.

What is going to happen with those findings if the temperature of bulk water is decreased from room temperature? Will the scale-invariant behaviour, detected for bulk

water at room temperature, be maintained at low temperature? We have found that the answer to this question is affirmative. Thus an analysis equivalent to that we have performed at room temperature shows the existence of a scale-free dynamics for bulk water at 243 K (see inset Fig. 9). An equivalent behaviour has been found for the intermediate temperatures 288, 273 and 258 K. In all cases the power law holds for at least three decades (0.1 – 100 ps). We have obtained a temperature independent exponent $\alpha = 0.58 \pm 0.09$. A power law behaviour along two decades (0.1 -10 ps), with a temperature independent exponent $\alpha = 0.5 \pm 0.1$, has also been described for bulk water for a particular bond lifetime distribution [74]. The molecular dynamics simulations were performed over 216 water molecules from room temperature down to 235 K. Please mind that although that power law exponent, $\alpha = 0.5 \pm 0.1$, nicely coincides with the value we have calculated from our data, $\alpha = 0.58 \pm 0.09$, the magnitudes under consideration are different (particular bond lifetime versus residence time).

3.4 Hydrogen bonds network

Since the special properties of water are extensively due to the particular singularity of its hydrogen-bonded network, a variable of remarkable interest would be the number of hydrogen bonds (n_{HB}) that a given water molecule at the biomolecule surface can establish with their neighbours. Thus we have considered the protein hydration water molecules that are linked to the biomolecule using this kind of interaction and calculated the number of hydrogen bonds that they establish with the protein and with the rest of the solvent. The average value is presented in Table 2 as a function of the temperature. That magnitude increases as the temperature decreases (from $n_{HB} = 3.32 \pm 0.02$ at 300 K to $n_{HB} = 3.50 \pm 0.02$ at 243 K). We have used standard geometrical criterion for the determination of the existence of a hydrogen bond between two atoms: the distance between donor and acceptor atoms within 0.35 nm and the hydrogen-donor-acceptor angle smaller than 30º [75]. This criterion will be used all along the work. As a consequence of that H-bond criterion, all the water molecules hydrogen bonded to the protein will be at a distance smaller than 0.35 nm from the biomolecule. In order to understand the referred augmentation of hydrogen bonds with cooling we have calculated the percentage of water molecules that present a given number of hydrogen bonds.

Thus a bulk water molecule taken as a reference can show different number of hydrogen bonds with its neighbours as a function of time. The coordination of the first hydration shell of a neat water molecule shows up to six hydrogen bonds at room and low temperature (1 to 5 within the error bar) [26,76]. In the case of the protein hydration water around the inhibitor barstar, water molecules with one, two, three, four and five hydrogen bonds per solvent molecule are detected at room and low temperature (see Fig. 10). The percentage of water molecules exhibiting 0 and 6 hydrogen bonds is negligible within the error bar. As cooling, the percentage of water molecules exhibiting 4 hydrogen bonds per water molecule, x^{HB4}, increases, while that of the rest of water molecules decreases. Considering those results it is not surprising that the average number of hydrogen bonds exhibited by solvent molecules hydrogen bonded to the biomolecule increases as temperature decreases, as mentioned in the previous paragraph. Interestingly the increase of an average tetrahedral order parameter, $\langle q_{tet} \rangle$, with decreasing temperature have been reported for trp-cage mini-protein hydration water [60,77]. That order parameter is an indication of the tetrahedral character of the

hydrogen bonding network (perfect thetrahedrality corresponds to q_t = 1). Moreover a distribution of the tetrahedral order parameter, $P(q_{tet})$, versus q_{tet} indicates that the probability of finding trp-cage hydration water molecules exhibiting high tetrahedral order increases with a decrease of temperature [60]. Please mind that although those results nicely coincide with ours, the water model used, the biomolecule and the thickness of the protein hydration water are different.

As commented above, the average number of hydrogen bonds that a water molecule exhibits within the hydration water of barstar, amounts n_{HB} = 3.32 ± 0.02 at 300 K (see Table 2). That value is smaller than previous experimental determinations for bulk water that report an average value of 3.5 hydrogen bonds per water molecule [78,79]. In order to understand that point and to test if this scenario also holds at low temperature, we have calculated the number of hydrogen bonds that a bulk water molecule of reference establishes with their neighbours. For performing those calculations, we have used all-atom molecular dynamics simulations carried out on neat water at room and low temperature [26], following the same simulation protocol than that used in the present work. As the temperature decreases that number of hydrogen bonds increases from n_{HB} = 3.46 ± 0.02 at room temperature up to n_{HB} = 3.74 ± 0.02 at 243 K approaching the ideal value of four (see Table 2, bulk water). It is not surprising that the average number of hydrogen bonds in the case of protein hydration water is smaller than that of bulk water, at room but also low temperature, since the percentage of water molecules exhibiting 4 hydrogen bonds per solvent molecule, x^{HB4}, is smaller for protein hydration water than for bulk water, at both room and low temperature (x^{HB4} = 38.9 ± 0.5 % versus x^{HB4} = 45.5 ± 0.5 % for biological water and neat water, respectively, at 300 K; x^{HB4} = 48.4 ± 0.5 % versus x^{HB4} = 59.8 ± 0.5 %, at 243 K), see Fig. 10. In both cases, protein hydration water and bulk water, the percentage of water molecules exhibiting coordination number different from 4 decreases with temperature.

In the previous paragraph we have presented a scenario calculated for all the protein hydration water molecules. Let now consider just one biological water molecule, a peculiar one as that shown in Fig. 7. That special solvent molecule exhibits significant long residence times within the protein hydration shell at room and low temperature (> 2 ns at 300 K and > 20 ns at 243 K, see section 3.2). We have calculated the average number of hydrogen bonds this water molecule establishes with the protein and with the solvent, as a function of time: 2.47 and 0.10, respectively, total number = 2.57 ± 0.02, at room temperature (300 K); and 2.37 and 0.22, total number = 2.59 ± 0.02, at low temperature (243 K). It is possible to conclude that nearly the totality of hydrogen bonds of that referred water molecule are established with the protein and not with the solvent, in both scenarios: room and low temperature. Then although for all the temperatures considered (300-243 K), we have calculated that the average of water molecules in the hydration shell of the protein establish more hydrogen bonds with the solvent (75 ± 1 %) than with the biomolecule (25 ± 1 %), this result does not preclude some particular water molecules from exhibiting the reverse situation: more hydrogen bonds with the protein than with the solvent, as shown in the case of the particular water molecule depicted in Fig. 7. Moreover since the number of hydrogen bonds that special molecule forms with the solvent is nearly cero, the possibilities of exchange with neighbouring water molecules are very small and therefore that slow water molecule has serious difficulties to escape from its particular position near the biomolecule. As a consequence, it exhibits especially long residence times within the protein hydration shell.

The temporal evolution of the number of hydrogen bonds associated to this peculiar water molecule is shown in Fig. 11 at atomic level. That figure shows that the number of hydrogen bonds that water molecule forms with the protein and the solvent, oscillates between 0 and 5 along the simulation time (1 and 4 considering error bars). We have also calculated the percentages of hydrogen bonds associated to those numbers. They are depicted in Fig. 10 at room (300 K) and low temperature (243 K). That figure shows that such a percentage does not much change with temperature, at least when compared with the data for the protein hydration solvent molecules that are also presented in the same figure for comparison. Moreover Fig. 10 shows that, in the case of that special solvent molecule, the maximum of the curves corresponds to an *x*-axis value of 3 hydrogen bonds per water molecule, with a negligible percentage associated to an *x*-axis value of 4 hydrogen bonds per water molecule. That hydrogen bonds distribution is not at all the case for an average solvent molecule of protein hydration water, as shown in Fig. 10. Those results clearly illustrate the particular scenario that special solvent molecule presents when compared with the average of protein hydration water molecules. A distribution of the tetrahedral order parameter, $P(q_{tet})$, versus q_{tet}, has been reported to depend on the particular examined area of the tenebrio molitor antifreeze protein at 220 K [80,81].

4. Discussion

In this section the results provided in section 3 are discussed within the frame of experimental and simulated data, as well as theoretical models, previously reported in the bibliography.

4.1 Diffusion-trap model

A dimensionless stretched exponential parameter $\beta = 0.48 \pm 0.01$ has been obtained in section 3.1 for the relaxation process of residence times of hydration water molecules at the surface of the protein barstar (see Table 1 and Fig. 3). As mentioned in that section, experimental results calculated for water at the surface of some other proteins show quantitative agreement with that result, at room but also at low temperature. In this section we propose an explanation for that particular value on the basis of the 'diffusion-trap' model [54]. That topological model was developed to understand electronic relaxation in amorphous semiconductors, where excitons diffuse to network defects. Within the 'diffusion-trap' model a distribution of excitations diffuse to traps where they disappear. The excitations that are near the traps are annihilated first and those that are located at higher distances take longer times to reach the traps. This kind of memory effect could be the origin of the stretched exponential decay reported in section 3.1.

The 'diffusion-trap' model predicts $\beta = 3/5$ for short-range forces but $\beta = 3/7$ for relaxation when long-range forces are present [54]. In the case of bulk water we have calculated the stretched exponent as $\beta = 0.59 \pm 0.01$ at room temperature [26]. That value is also valid as the temperature decreases down to 243 K [26]. Then the relaxation process that takes place in liquid bulk water, at ambient and low temperature, is determined by short-range molecular decay channels. However a stretched exponent $\beta =$

0.48 ± 0.01 (see Table 1 and Fig. 3) would indicate that are long-range interactions which dominates the relaxation dynamics of protein hydration water. Therefore it is possible to conclude that relaxation processes associated to residence times of water molecules in the hydration shell of the protein are mainly governed by long-range interactions, in opposition to short-range forces associated to this type of relaxation in bulk water.

Within the diffusion-trap model, the dependence of the stretched exponent β with d_{eff} follows the expression $\beta = d_{\mathrm{eff}}/(d_{\mathrm{eff}} + 2)$, where d_{eff} is the effective dimensionality of the pathways involved in the excitations decay. Since in our case $\beta = 0.48 \pm 0.01$ therefore $d_{eff} \approx 1.8$. The protein hydration water molecules form a quasi-two-dimensional connected hydrogen bond network around the biomolecule. Interestingly enough, in the case of bulk water d_{eff} has been calculated as 2.9, suggesting a quasi-three-dimensional effective pathway of the excitations decay (relaxation of residence times) [26]. In addition the independence of the stretched exponent with temperature, shown in Table 1 and Fig. 3, would indicate that the nature of the relaxation process, reflected by β, does not change when the hydration water of that protein is cooled down from ambient to 243 K. Moreover that explanation based on the 'diffusion-trap' model can be also applied to the temperature independent result $\beta = 0.5$ reported from neutron scattering experiments performed on the hydration water at the surface of some other proteins [35,57].

4.2 Scale-invariant dynamics

A power law temporal distribution showing scale-free dynamics has been found to take place at the first hydration layer of the protein barstar (see section 3.3). Power law distributions exhibit a ubiquitous appearance in different research fields [82-84]. Thus, in physics, they are commonly associated to the occurrence of critical phenomena as phase transitions [85]. Generic mechanisms have been proposed to clarify such ubiquity. Power law dependences showing scale-invariance have been explained in terms of purely stochastic multiplicative processes or in terms of a model based on the combination of stochastic reaction like events and a diffusion process, which leads to the development of intermittency patterns [86,87]. Self-organization models apply to large dynamical systems that organize themselves into a state far out of equilibrium with propagating activity of all sizes [83,88]. The macroscopic behaviour of those systems display the spatial and/or temporal scale-invariance characteristic of the critical point of a phase transition, but without the need to tune control parameters to a precise value. This is because the system, effectively, evolves itself towards criticality. In a self-organized critical state, the number of large-size events is related to the number of small-size events by a scale-free power law, as we have shown to occur for bulk and protein hydration water (see section 3.3)

The fact that not only protein hydration water but also bulk water exhibit a scale-free behaviour, with respect to the residence times of solvent molecules, give rise to a point of reflexion considering the dynamics of water around biomolecules. Thus some authors state that the heterogeneous scenario biological water presents is due to the heterogeneity of the protein surface itself in contrast to the more homogeneous nature of the solvent [30]. A protein surface is highly heterogeneous presenting different amino acid residues of diverse polar character. Thus water molecules close to the protein sense different scenarios from point to point of the surface. On the other hand our results

shown that bulk water also shows a heterogeneous dynamical behaviour. Therefore it can be concluded that not only the protein is responsible of the heterogeneous scenario protein hydration water presents but also the solvent. Biological water sees both 'scenarios' and tries to adapt to them since the three entities must coexist at the same time. Thus the dynamics that special water exhibits would be the result of a compromise between the dynamics of both protein and bulk water. In other words, both dynamics would couple through the intermediation of biological water. That scenario holds not only at room but also at low temperature.

4.3 Freezing protein hydration water?

The number of hydrogen bonds, per solvent molecule, associated to the hydration water of barstar at the lowest temperature considered, n_{HB} = 3.50 ± 0.02 at 243 K (see Table 2), is smaller than the number of hydrogen bonds, per solvent molecule, for bulk water at its freezing point of 273 K (n_{HB} = 3.59 ± 0.02, see Table 2). That occurs because the number of water molecules exhibiting 4 hydrogen bonds per water molecule, is smaller for protein hydration water at 243 K than for bulk water at 273 K (x^{HB4}= 48.4 ± 0.5 % and x^{HB4} = 53.8 ± 0.5 %, respectively), see Fig. 10. That result suggests a quantitative explanation for the following experimental finding: biological water keeps liquid at temperatures well below the freezing point of bulk water, in fact it does not freeze until the temperature is well below that temperature [89-92]. When cooling below 273 K, protein hydration water would not freeze because it would not exhibit a sufficiently high enough percentage of water molecules presenting 4 hydrogen bonds. The crossover could be established at $x_c^{HB4} \approx 54$ % (percentage of water molecules presenting 4 hydrogen bonds in bulk water at 273 K). Above that crossover concentration x_c^{HB4} water would freeze, below it would not. That particular scenario helps to preserve life under temperature extreme conditions (bio-cryopreservation).

4.4 Protein hydration water transition and bioactivity: water defects

In this section we discuss an origin for the protein hydration water transition at T_L = 226 ± 4 K (see section 3.1) within the frame of the 'diffusion-trap' model [54] and the 'cage effect' [93,94]. In section 3.4 the number of hydrogen bonds that water molecules establishes with the protein barstar and the solvent have been calculated. Water molecules with one, two, three, four and five hydrogen bonds per solvent molecules are detected at room and low temperature (see Fig. 10). All-atoms molecular dynamics simulations of hydrogen bonding in bulk water have found water molecules with up to six hydrogen bonds (five within the error bar) [26]. Moreover experimental evidences for isolated water suggest that the ideal tetrahedral network is not perfect but contains 'defects' such an extra (fifth) molecule in the first coordination shell [95,96]. The two alone non-bonding pairs of electrons interact not with two, as expected from a perfect tetrahedral coordination, but with three protons from three different molecules. These 'defects' would be caused by an increase/reduction of molecules with respect to a tetrahedral coordination.

The 'diffusion-trap' model considers a uniform distribution of excitations that diffuse to traps where the excitations are annihilated [54]. It sounds reasonable to propose that in the case of protein hydration water, molecules with a coordination number higher than 4 could act as excitons while solvent molecules with a coordination number lower than 4 could behave as traps. The number of solvent molecules at barstar surface that

exhibit four hydrogen bonds per water molecule, increases as the temperature decreases, x^{HB4} = 38.9 ± 0.5 % at 300 K versus x^{HB4} = 48.4 ± 0.5 % at 243 K (see Fig. 10). Thus in the case of protein hydration water the number of 'defects' ('excitons' and 'traps') decreases on cooling. That effect has been also observed in bulk water (x^{HB4} = 45.5 ± 0.5 % at 300 K versus x^{HB4} = 59.8 ± 0.5 % at 243 K, see Fig. 10) [26]. As temperature goes down the number of hydrogen bonds exhibited by an average solvent molecule of neat water increases approaching a more perfect tetrahedral hydrogen bond network.

The increase of the decay time τ on cooling is the fingerprint of the protein hydration water transition occurring at $T_L \approx 225$ K (see section 3.1). On the other hand the augmentation of τ as the temperature decreases, shown by protein hydration water (see section 3.1), can be interpreted considering the dependence of the 'defects' with temperature together with the 'cage effect' [93,94], i.e. the confinement of molecules due to the interactions with neighbouring solvent molecules. Thus considering a tagged particle, if the other liquid particles were fixed, the tagged one could not move very far. It would be confined in a cage formed by its neighbours. It can migrate only through rearrangement of the particles surrounding it. Therefore as the number of 'defects' decreases on cooling (see above), a given water molecule will be longer confined in its cage due to a higher number of neighbours presenting tetrahedral, and then more stable, coordination. Since the relaxation time τ would be related to the lifetime of the cage, larger τ values would be expected for protein hydration water as the temperature goes down due to a decrease on the number of 'hydrogen bond defects'.

In this paragraph we discuss an origin for the protein dynamical transition occurring at $T_p \approx 225$ K [34] and a parameter determining protein bioactivity. Tarek and Tobias have shown that a complete structural relaxation of the protein requires relaxation of the water-protein hydrogen bond network via solvent translational displacement [97]. The translational diffusion of water molecules on a protein surface promotes the large-amplitude motion of proteins that are required for their biological activity [98]. Moreover Tarek and Tobias have also shown that inhibiting the solvent translational mobility (protein-water hydrogen bond dynamics) is dynamically analogous to dehydrating the protein [97]. Therefore since the decay time of protein hydration water τ tends to infinite below the dynamical transition at ~ 225 K (see section 3.1), the protein structural relaxation time is also going to be notably affected (dynamics tends to zero) below that temperature. That outcome can provide an origin for the dynamical transition proteins exhibit at 225 K and the severe decrease of its bioactivity below that temperature. Thus these two experimental findings can be explained by the decrease of 'hydrogen bond defects' in the protein hydration shell as temperature goes down. Therefore a relevant property of water to account for protein dynamical transition and protein bioactivity would be 'hydrogen bond defects'. If most of the protein hydration water molecules would present a tetrahedral arrangement (nearly no 'hydrogen bond defects'), the bioactivity of proteins would be negligible.

Considering future work, although the global dynamics of protein hydration water does not significantly change from one protein to another (see sections 1 and 3, and references therein), it would be of interest to compute the temperature dependence of the number of such 'hydrogen bonds defects' in the case of some other proteins and biomolecules different from barstar.

5. Conclusions

In this work the dynamics of the hydration shell of the protein barstar is analysed at low temperature (300 – 243 K) and compared with bulk water data. The results have been also discussed within a scenario constituted by various proteins as lysozyme, c-phycocyanin, myoglobin, green fluorescent protein, trp-cage or tenebrio molitor antifreeze protein, and are in quantitative agreement with experimental data (β, T_L, α and n_B).

The low temperature relaxation of residence times of water molecules in the protein hydration shell follows a stretched exponential function $exp[- (t / \tau)^{\beta}]$. The value of the stretched exponent $\beta = 0.48 \pm 0.01$ also support the existence of significant temporal disorder in the system and multiple decay time scales. The decay process is mainly dominated by long-range molecular relaxation channels, in opposition to the result obtained for bulk water (short range interactions). The independence of β with temperature suggests that this mechanism applies not only at ambient but also at low temperature within the range considered (300 – 243 K). As temperature decreases, the relaxation time τ increases, showing a divergence at a transition temperature $T_L = 226 \pm 4$ K. The distribution of residence times in the protein hydration water quantitatively indicates that not only the biomolecule is responsible for the heterogeneous scenario biological water presents but also the solvent.

The percentage of water molecules exhibiting 4 hydrogen bonds, x^{HB4}, is found to be essential for understanding some room and low temperature dependent properties of the protein hydration shell, suggesting an explanation for the unfreezing of protein hydration water as temperature reduces below 273 K (too low x^{HB4} value when compared with that of bulk water at that temperature). The dynamical transition that proteins and their hydration water exhibit at ~225 K would be explained by the decrease of hydrogen bond defects in the protein hydration shell as temperature goes down. If most of protein hydration water molecules would present a tetrahedral arrangement (nearly no 'hydrogen bond defects'), the bioactivity of proteins would be negligible.

Conflicts of interest

There are no conflicts to declare.

Acknowledgements

This work was funded by the Spanish Ministerio de Economia, Industria y Competitividad, and by the European Regional Development Fund (ERDF), under project FIS2017-87519-P. Financial support though grant E36_17R (Gobierno de Aragón, Spain) to Research Group FENOL is also acknowledged.

References

1. L. Bierdermannova, B. Schneider, Biochim. Biophys. Acta 1860 (2016) 1821-1835.
2. A. C. Fogarty, E. Duboué-Dijon, F. Sterpone, J. T. Hynes, D. Laage, Chem. Soc. Rev. 42 (2013) 5672-5683.
3. B. Bagchi, '*Water in biological and chemical processes*', Cambridge University Press, Cambridge, U.K. (2013) pp. 1-356.
4. S. Mondal, S. Mukherjee, B. Bagchi, J. Phys. Chem. Lett. 8 (2017) 4878-4882.
5. B. Bagchi, Proc. Natl. Acad. Sci. U. S. A. 113 (2016) 8355-8357.
6. M. Gupta, P. Khatua, C. Chakravarty, S. Bandyopadhyay, J. Phys. Chem. B 122 (2018) 1560-1572.
7. F. Mallamace, C. Corsaro, D. Mallamace, P. Baglioni, H. E. Stanley, S. H. Chen, J. Phys. Chem. B 115 (2011) 14280-14294.
8. S. Bandyopadhyay, S. Chakraborty, B. Bagchi, J. Am. Chem. Soc. 127 (2005) 16660-7.
9. M. Grossman, B. Born, M. Heyden, D. Tworowski, G. Fields, L. Sagi, M. Havenith, Nat. Struct. Mol. Biol. 18 (2011) 1102-8.
10. R. K. Eppler, R. S. Komor, J. Huynh, J. S. Dordick, J. A. Reimer, D. S. Clark*, Proc. Natl. Acad. Sci. U. S.* A., 103 (2006) 5706-5710.
11. P. Khatua, J. C. Jose, N. Sengupta, S. Bandyopadhyay, Phys. Chem. Chem. Phys. 18 (2016) 30144-30159.
12. E. Mamontov, X. Q. Chu, Phys. Chem. Chem. Phys. 14 (2012) 11573-11588.
13. D. Laage, T. Elsaesser, J. T. Hynes, Chem. Rev. 117 (2017) 10694-10725.
14. M. C. Beliissent-Funel, A. Hassanali, M. Havenith, R. Henchman, P. Pohl, F. Sterpone, D. van der Spoel, Y. Xu, A. E. Garcia, Chem. Rev. 116 (2016) 7673-7697
15. P. Ball, Proc. Natl. Acad. Sci. U. S. A. 114 (2017) 13327-13335.
16. Y. Levy, J. N. Onuchic, Annu. Rev. Biophys. Biomol. Struct. 35 (2006) 389-415.
17. S. Kiihne, R. G. Bryant, Biophys. J. 78 (2000) 2163-2169.
18. A. C. Fogarty, D. Laage, J. Phys. Chem. B 118 (2014) 7715-7729.
19. F. Sterpone, G. Sirnemann, D. Laage, J. Am. Chem. Soc. 134 (2012) 4116-4119.
20. T. Li, A. A. Hassanali, Y. T. Kao, D. Zhong, S. J. Singer, J. Am. Chem. Soc. 129 (2007) 3376-3382.
21. Z. F. Brotzakis, C. C. M. Groot, W. H. Brandeburgo, H. J. Bakker, P. G. Bolhuis, J. Phys. Chem. B 120 (2016) 4756-4766.
22. K. E. Furse, S.A. Corcelli, J. Phys. Chem. Lett. 1 (2010) 1813-1820.
23. L. Nilsson, B. Halle, Proc. Natl. Acad. Sci. USA, 102 (2005) 13867-13872.
24. K. Sahu, S. K. Mondal, S. Ghosh, K. Bhattacharyya, Bull. Chem. Soc. Jpn. 80 (2007) 1033-1043.
25. M. C. Morón, Phys. Chem. Chem. Phys. 14 (2012) 15393-15399.
26. M. C. Morón, D. Prada-Gracia, F. Falo, Phys. Chem. Chem. Phys. 18 (2016) 9377-9387.
27. B. Bagchi, Chem. Phys. Lett. 529 (2012) 1-9.
28. A. Bizzarri, S. Cannistraro, J. Phys. Chem. B 106 (2002) 6617-6633.
29. E. Duboue-Dijon, A. C. Fogarty, D. Laage, J. Phys. Chem. B 118 (2014) 1574-1583.
30. P. K. Nandi, J. J. Enblish, Z. Futera, A. Benedetto, Phys. Chem. Chem. Phys. 19 (2017) 318-239.
31. S. Cerveny, F. Mallamace, J. Swenson, M. Vogel, L. Xu, Chem. Rev., 116 (2016) 7608-7625.

32. F. Mallamace, C. Corsaro, D. Mallamace, S. Vasi, C. Vasi, H. E. Stanley, S. H. Chen., J. Chem. Phys. 142 (2015) 215103.
33. X. Q. Chu, A. Faraone, C. Kim, E. Fratini, P. Baglioni, J. B. Leao, S. H. Chen, J. Phys. Chem. B Lett. 113 (2009) 5001-5006.
34. F. Mallamace, C. Corsaro, D. Mallamace, N. Cicero, S. Vasi, G. Dugo, H. E. Stanley, Front. Phys. 10 (2015) 106104.
35. S. H. Chen, L. Liu, E. Fratini, P. Baglioni, A. Faraone, E. Mamontov, Proc. Natl. Acad. Sci. U. S. A., 103 (2006) 9012-9016.
36. M. Hoefling, K. E. Gottschalk, J. Struct. Biol. 171 (2010) 52-63.
37. M. P. Nikitin, T. A. Zdobnova, S.V. Lukash, O. A. Stremovskiy, S. M. Deyev, Proc. Natl. Acad. Sci. USA, 107 (2010) 5827-5832.
38. A. Sekhar, J. B. Udgaonkar, Biochemistry 50 (2011) 805-819.
39. H. F. M. C. Martiniano, N. Galamba, J. Phys. Chem. B 117 (2013) 16188-16195.
40. P. Dutta, M. Botlani, S. Varma, J. Phys. Chem. B 118 (2014) 14795-14807.
41. D. Van der Spoel, E. Lindahl, B. Hess, G. Groenhof, A. E. Mark, H. J. C. Berendsen, J. Comput. Chem. 26 (2005) 1701-1718.
42. H. J. C. Berendsen, D. van der Spoel, R. van Drunen, Comput. Phys. Commun. 91 (1995) 43-56.
43. W. L. Jorgensen, D. S. Maxwell, J. Tirado-Rives, J. Am. Chem. Soc. 118 (1996) 11225-36.
44. E. K. Watkins, W. L. Jorgensen, J. Phys. Chem. A 105 (2001) 4118-4125.
45. B. Hess, H. Bekker, H. J. C. Berendsen, J. G. E. M.Fraaije, J. Comput. Chem. 18 (1997) 1463-1472.
46. H. J. C. Berendsen, J. P. M. Postma, W. F. vanGunsteren, J. Hermans, in *Intermolecular Forces,* ed B. Pullman, Reidel Publishing Company, Dordrecht, The Netherlands (1981) pp 331-342.
47. N. Choudhury, J. Phys. Chem. C 111 (2007) 2565-2572.
48. D. J. Tobias, N. Sengupta, M. Tarek, Faraday Discuss. 141 (2009) 99-116.
49. J. E. Curtis, T. E. Dirama, G. A. Carri, D. J. Tobias, J. Phys. Chem. B Lett. 110 (2006) 22953-22956.
50. F.W. Starr, S. Harrington, F. Sciortino, H. E. Stanley, Phys. Rev. Lett. 82 (1999) 3629-3632.
51. A. Taschin, P. Bartolini, A. Marcelli, R. Righini, R. Torre, Faraday Discuss. 167 (2013) 293-308.
52. G. Williams, D. C. Watts, Trans. Faraday Soc. 66 (1970) 80-85.
53. R. Kohlrausch, Ann. Phys. (Leipzig) 148 (1847) 353-405.
54. J. C. Phillips, Rep. Prog. Phys. 59 (1996) 1133-1207.
55. R. Torre, P. Bartolini, R. Righini, Nature 428 (2004) 296-299.
56. D. C. Johnston, Phys. Rev. B 74 (2006) 184430.
57. S S. Dellerue, M. C. Bellissent-Funel, Chem. Phys. 258 (2000) 315-325.
58. A. Faraone, L. Liu, C. Y. Mou, C. W. Yen, S. H. Chen, J. Chem. Phys. 121 (2004) 10843-1 0846.
59. M. Lagi, X. Chu, C. Kim, F. Mallamace, P. Baglioni, S. H. Chen, J. Phys. Chem. B Lett. 112 (2008) 1571-1575.
60. M. Gupta, C. Chakravarty, S. Bandyopadhyay, J. Chem. Theory Comput. 12 (2016) 5643-5655.
61. K. Bhattacharyya, Chem. Commun. 25 (2008) 2848-2857.
62. B. Bagchi B, B. Jana, Chem. Soc. Rev. 39 (2010) 1936-1954.
63. S. K. Pal, J. Peon, B. Bagchi, A. H. Zewail, J. Phys. Chem. B 106 (2002) 12376-12395.

64. Y. Xu, R. Gnanasekaran, D. M. Leitner, Chem. Phys. Lett. 564 (2013) 78-82.
65. R. Gnanasekaran, Y. Xu, D. M. Leitner, J. Phys. Chem. B 114 (2010) 16989-16996.
66. K. Chakraborty, S. Bandyopadhyay, J. Chem. Phys. 143 (2015) 045106.
67. R. G. Palmer, D. L. Stein, E. Abrahams, P. W. Anderson, Phys. Rev. Lett. 53 (1984) 958-961.
68. P. Bak, C. Tang, K. Wiesenfeld, Phys. Rev. A 38 (1988) 364-374.
69. R. Albert, A. L. Barabasi, Rev. Mod. Phys. 74 (2002) 47-97.
70. D. M. Leitner, Annu. Rev. Phys. Chem. 59 (2008) 233-259.
71. X. Yu, D. M. Leitner, J. Chem. Phys., 119 (2003) 12673-12679.
72. J. Sancho, Cell. Mol. Life Sci. 63 (2006) 855-864.
73. S. Boccaletti, V. Latora, Y. Moreno, M. Chavez, D. U. Hwang, Phys. Rep. 424 (2006) 175-308.
74. F. Sciortino, P. H. Poole, H. E. Stanley, S. Havlin, Phys. Rev. Lett. 64 (1990) 1686-1689.
75. M. Jana, S. Bandyopadhyay, J. Chem. Phys. 134 (2011) 025103.
76. G. Sutmann, R. Vallauri, J. Mol. Liq. 98-99 (2002) 213-224.
77. M. Gupta, D. Nayar, C. Chakravary, S. Bandyopadhyay, Phys. Chem. Chem. Phys. 18 (2016) 32796-32813.
78. T. M. Raschke, Curr. Opin. Struc. Biol. 16 (2006) 152-159.
79. B. Bagchi, Chem. Rev. 105 (2005) 3197-3219.
80. U. S. Midya, S. Bandyopadhyay, Langmuir 33 (2017) 5499-5510.
81. U. S. Midya, S. Bandyopadhyay, J. Phys. Chem. B 118 (2014) 4743-4752.
82. M. Schroeder, *Fractal, Chaos, Power Laws*, Freeman, New York (1991).
83. P. Bak, C. Tang, K. Wiesenfeld, Phys. Rev. Lett. 59 (1987) 381-384.
84. P. Bak, *How Nature Works*, Springer-Verlag, New York (1996).
85. C. N. R. Rao, K. J. Rao, *Phase transitions in solids*, McGraw-Hill, New York (1977).
86. D. H. Zanette, S. C. Manrubia, Phys. Rev. Lett. 79 (1997) 523-526.
87. S. C. Manrubia, D. H. Zanette, Phys. Rev. E 58 (1998) 295-302.
88. M. Paczuski, S. Maslov, P. Bak, Phys. Rev. E 53 (1996) 414-443.
89. F. Alvarez, A. Alegria, J. Comenero, *Phys. Rev. B* 44 (1991) 7306-7312.
90. V. Velikov, S. Borick, C. A. Angell, Science 294 (2001) 2335-2338
91. N. Giovambattista, C. A. Angell, F. Sciortino, H. E. Stanley, Phys. Rev. Lett. 93 (2004) 47801.
92. S. Cerveny, G. A. Schwartz, R. Bergman, J. Swenson, Phys. Rev. Lett. 93 (2004), 245702.
93. A. Angell, Nature, 393 (1998) 521-524.
94. W. Gotze, L. Sjogren, Chem. Phys. 212 (1996) 47-59.
95. N. Giovambattista, F. W. Starr, F. Sciortino, V. Buldyrev, H. E. Stanley, Phys. Rev. E 65 (2002) 041502.
96. F. Sciortino, A. Geiger, H. E. Stanley, Nature, 354 (1991) 218-221.
97. M. Tarek, D. J. Tobias, Phys. Rev. Lett. 88 (2002) 138101.
98. G. Schirò, Y. Fichou, F. X. Gallat, K. Wood, F. Gabel, M. Moulin, M. Härtlein, M. Heyden, J. P. Colletier, A. Orecchini, A. Paciaroni, J. Wuttke, D. J. Tobias, M. Weik, Nat. Commun. 6 (2015) 6490.

Figures.

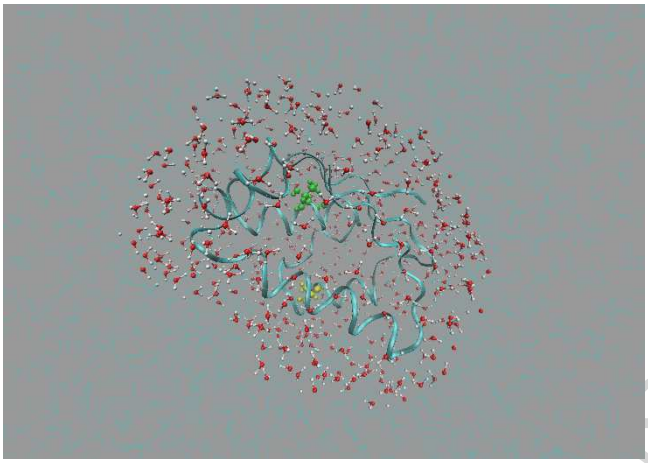

Fig. 1. The protein barstar and its hydration water molecules situated at a distance smaller than 0.40 nm from the biomolecule. The residues Alanine36 and Threonine19 (section 3.2) are depicted in yellow and green, respectively. The figure has been drawn using the VMD software (W. Humphrey, A. Dalke, K. Schulten, 'VMD - Visual Molecular Dynamics', J. Molec. Graphics 14 (1996) 33-38).

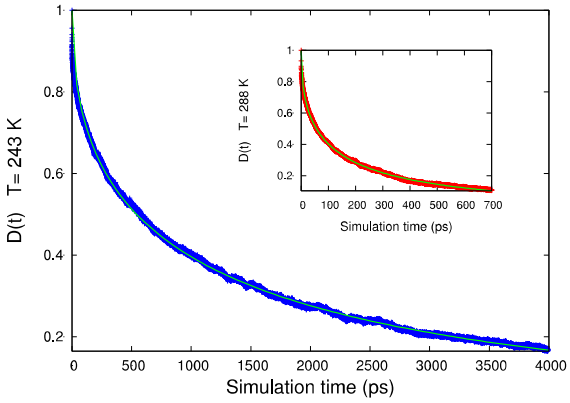

Fig. 2. Relaxation process for water in the first hydration shell of the inhibitor barstar. $D(t)$ represents the number of water molecules that remain at a distance smaller than 0.40 nm from the protein at a given time t with respect to that number at the initial time (see section 3.1). The symbols are data points obtained from molecular dynamics simulations at 243 and 288 K (inset). The continuous line represents the best fit using a stretched exponential function $exp[- (t / \tau)^{\beta}]$. See section 3.1 and Table 1 for additional information.

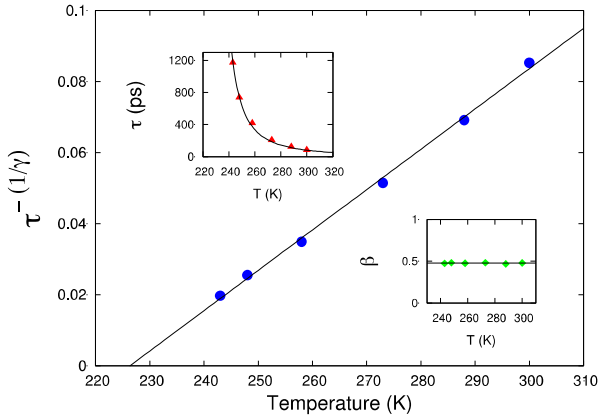

Fig. 3. Decay dynamics for the first hydration shell of the inhibitor barstar cooled from 300 K down to 243 K. The magnitude τ is the effective relaxation time obtained from the fit of the molecular dynamics simulations data to a stretched exponential function $exp[- (t / \tau)^{\beta}]$. The temperature independence of the exponent β is also shown (inset below). The straight line, in the main body of the figure, illustrates the power-law divergence $\tau \sim (T - T_L)^{-\gamma}$ with best fit for $T_L = 226 \pm 4$ K and $\gamma = 1.8 \pm 0.2$. See Fig. 2, Table 1 and sections 3.1, 4.1 and 4.4 for details.

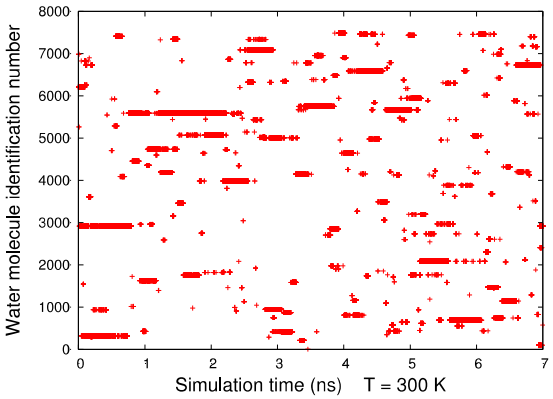

Fig. 4. Snapshot showing the heterogeneous distribution of residence times for water molecules located at a distance smaller than a cutoff of 0.40 nm from the oxygen atom (carboxyl group) within the non-polar residue Alanine36 of the inhibitor barstar. The data corresponds to room temperature at T= 300 K. If at a particular time of the simulation (*x*-coordinate), a given water molecule (*y*-coordinate) is located at a distance of the protein smaller than the cutoff, then a cross appears at the corresponding (*x*,*y*) location. If the distance is higher or equal than the cutoff, a blank is settled instead. The length of the lines inside the figure provides the value of the resident time t_r for each water molecule. In some cases, the lines reduce to a single point. The presence of multiple time scales can be clearly seen at this atomic level. Data calculated using the GROMACS software package. See section 3.2 for details.

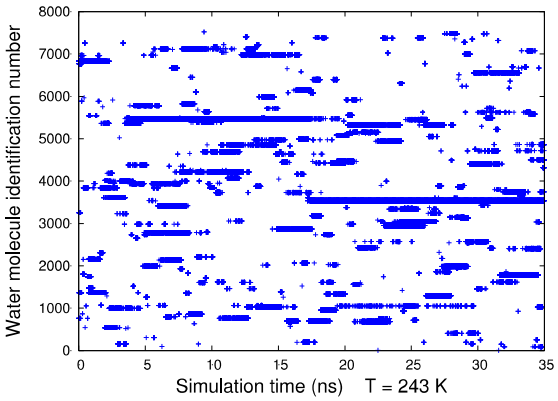

Fig. 5. Snapshot showing the heterogeneous distribution of residence times for water molecules located at a distance smaller than a cutoff of 0.40 nm from the oxygen atom (hydroxyl group) within the polar residue Threonine19 of the inhibitor barstar. The data corresponds to T= 243 K. If at a particular time of the simulation (*x*-coordinate), a given water molecule (*y*-coordinate) is located at a distance of the protein smaller than the cutoff, then a cross appears at the corresponding (*x*,*y*) location. If the distance is higher or equal than the cutoff, a blank is settled instead. The length of the lines inside the figure provides the value of the resident time t_r for each water molecule. In some cases, the lines reduce to a single point. The presence of multiple time scales can be clearly seen at this atomic level. Data calculated using the GROMACS software package. See section 3.2 for additional information.

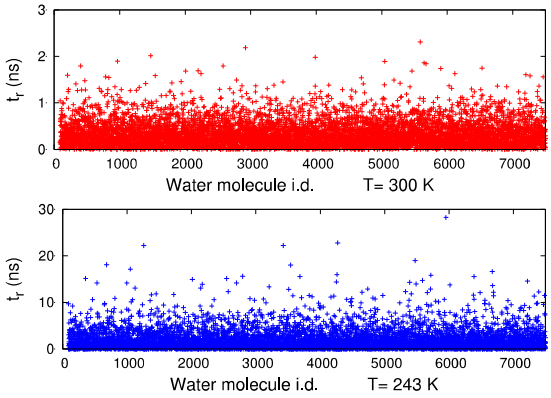

Fig. 6. Residence times (t_r) of water molecules located at a distance smaller than a cutoff of 0.40 nm from the protein surface. The figure shows that the maximum value of those residence times increases one order of magnitude when water is cooled from 300 K (upper part of the figure) down to 243 K (lower part). Please mind the *y*-axis scaling in both cases (upper and lower representations). See section 3.2 for details.

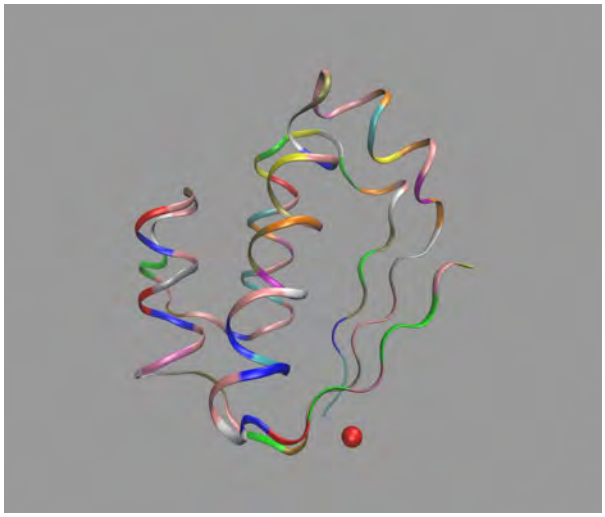

Fig. 7. The inhibitor barstar and one of the slowest water molecules exhibiting larger residence times within its hydration shell. That solvent molecule spends more than 2 ns at room temperature (300 K) and more than 20 ns at low temperature (243 K) in the pocket defined by the residues Pro48, Leu49, Val50, Asp83, Ile84 and Thr85 of the protein. The figure has been drawn using the VMD software. See sections 3.2 and 3.4 for additional information.

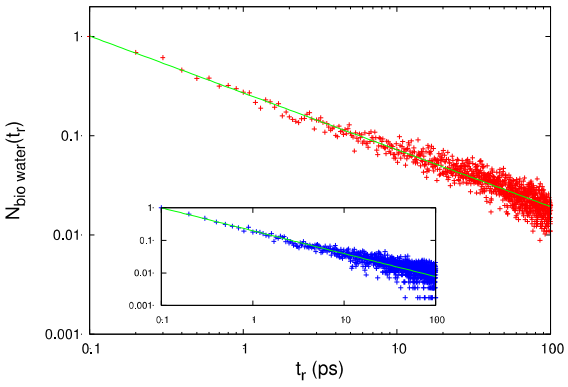

Fig. 8. Normalized number of water molecules (*y*-axis) that spend a time t_r (*x*-axis) within a cutoff of 0.40 nm from the protein surface. Both axes are in logarithmic scale. The symbols are data points obtained from molecular dynamics simulations performed on protein hydration water at 288 K (curve above) and 243 K (inset below). The straight lines represent the best fit to a power law distribution $t_r^{-\alpha}$ ($\alpha = 0.63 \pm 0.07$). This figure shows that protein hydration water displays the same type of distribution at any scale, i.e., it presents a scale-free dynamics (with respect to the residence time of solvent molecules t_r). See sections 3.3 and 4.2 for details.

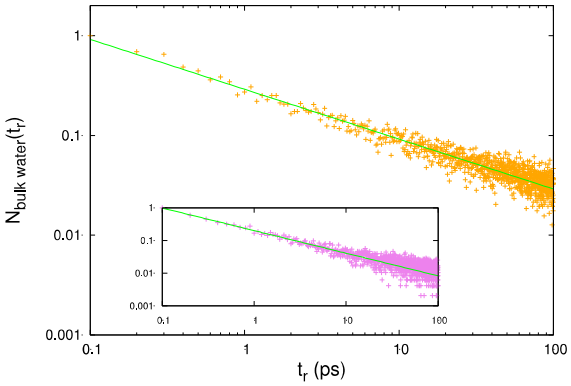

Fig. 9. Normalized number of water molecules (*y*-axis) that spend a time t_r (*x*-axis) within a sphere of solvent molecules with a radius of 2.0 nm. Both axes are in logarithmic scale. The symbols are data points obtained from molecular dynamics simulations performed on bulk water at 300 K (curve above) and 243 K (inset below). The straight lines represent the best fit to a power law distribution $t_r^{-\alpha}$ ($\alpha = 0.58 \pm 0.09$). This figure shows that bulk water displays the same type of distribution at any scale, i.e., it presents a scale-free dynamics (with respect to the residence time of solvent molecules t_r). See sections 3.3 and 4.2 for details.

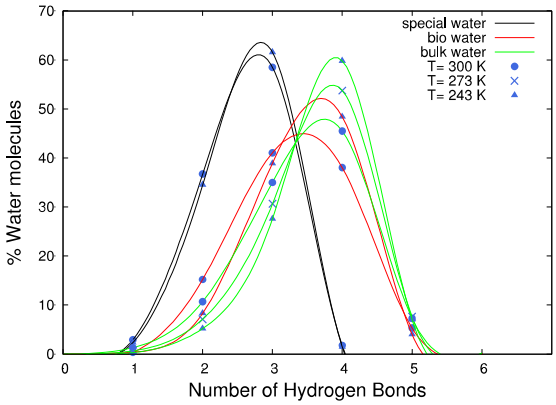

Fig. 10. Percentage of water molecules as a function of the number of hydrogen bonds they exhibit. 'Bio water' refers to the average calculated over all the water molecules hydrogen bonded to the protein. 'Special water' refers to a particular molecule exhibiting exceptional long residence times within the hydration shell of the protein (more than 2 ns at room temperature and more than 20 ns at low temperature (243 K), see Fig. 7). The data corresponding to bulk water at 300 and 243 K are taken from reference [26]. Lines are eye-guides. For additional information, see sections 3.2, 3.4, 4.3 and 4.4.

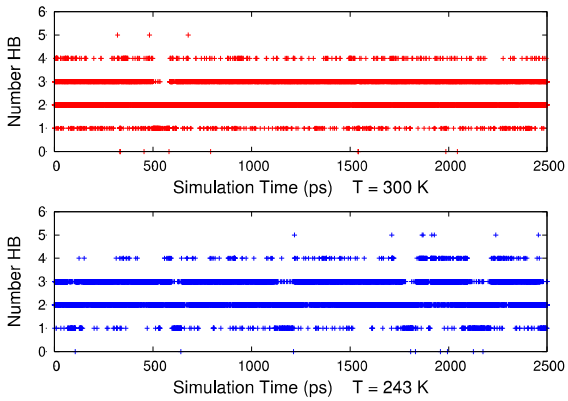

Fig. 11. Number of hydrogen bonds, as a function of simulation time, that a special protein hydration water molecule establishes with the biomolecule and the solvent at room and low temperatures (300 and 243 K). That water molecule shows significant long residence times in one pocket of the protein barstar (more than 2 ns at 300 K and more than 20 ns at 243 K). Data calculated using the GROMACS software package. See section 3.2, 3.4 and Fig. 7 for additional information.

Table 1. Relaxation phenomena. Ambient and low temperature stretched exponential parameters calculated for water molecules located at a distance smaller than 0.40 nm from the protein barstar. See section 3.1.

T (K)	τ (ps)	β
300 ± 1	84 ± 1[a]	0.48 ± 0.01[a]
288 ± 1	123 ± 1	0.47 ± 0.01
273 ± 1	209 ± 2	0.48 ± 0.01
258 ± 1	419 ± 4	0.48 ± 0.01
248 ± 1	737 ± 7	0.48 ± 0.01
243 ± 1	1173 ± 9	0.47 ± 0.01

[a] Ref. [25]

Table 2. Number of hydrogen bonds (n_{HB}), as a function of the temperature, an average water molecule establishes with its neighbours. 'n_{HB} bio water' corresponds to an average water molecule hydrogen bonded to the protein barstar. In this case the total number of hydrogen bonds (solvent-protein + solvent-solvent), per water molecule, are shown. 'n_{HB} bulk water' corresponds to an average water molecule in neat water. See section 3.4.

T (K)	n_{HB} bio water	n_{HB} bulk water
300 ± 1	3.32 ± 0.02	3.46 ± 0.02
288 ± 1	3.35 ± 0.02	3.53 ± 0.02
273 ± 1	3.38 ± 0.02	3.59 ± 0.02
258 ± 1	3.48 ± 0.02	3.67 ± 0.02
243 ± 1	3.50 ± 0.02	3.74 ± 0.02

Highlights

- The highly heterogeneous nature of low temperature protein hydration water dynamics is analysed through relaxation phenomena.
- Protein hydration water would not freeze at ~273 K due to its too low number of hydrogen bonds.
- Protein hydration water dynamical transition at ~225 K would occur due to the decrease of hydrogen bond defects with temperature.
- The bioactivity of proteins would be negligible without hydrogen bond defects in their hydration water.
- Low temperature protein hydration water presents a scale-free dynamics, surprisingly bulk water also does.